Turkish Journal of Computer and Mathematics Education *Vol.13 No.02 (2022), 748-760*

Research Article

A New Detection Method of IGBTs Open-Circuit Faults in an Induction Motor Drive

[a]Hicham Zaimen , [b]Ali Rezig , [c]Said Touati

[a]Assistant Professor, Department of Electrical Engineering, University MCM of Souk-Ahras, Algeria.
[b] Professor, Department of Electrical Engineering, University Mohamed SeddikBenyahia, Jijel, Algeria.
[c]Expert Researcher,Nuclear Research Center of Birine CRNB, BP 180, Aïn Oussera, Djelfa, Algeria.

Abstract: Due to the growing demand for the reliability and safety of industrial systems such as induction motor drives (IMDs), it is mandatory to detect all types of potential faults as early as possible to implement a fault-tolerant operation that minimizes the degradation of the performances and avoids dangerous situations. This paper presents a new fault detection and identification (FDI) method applied to an induction motor drive in the case of open IGBTs faults of a three-phase voltage source inverter (VSI). The diagnosis method of the open switch faults proposed in this work is based on the average absolute values of the normalized phase currents. This diagnosis method has some advantages in terms of fast fault detection time, robustness against transients, and it does not require extra hardware and sensors. The effectiveness of the proposed FDI method is verified through computer simulation using MATLAB-SIMULINK software.

Keywords: Induction motor drive, Field-oriented control, Fault diagnosis, Open switch fault, Voltage source inverter.

1. Introduction

At present, reliability, safety, and service continuity are major concerns in the field of AC variable speed drives. The induction motors (IMs) are now broadly used in different industrial and commercial applications. The reason for its massive use can mainly be attributed to its high reliability and durability, simplicity in design, cost-effectiveness, and operation at wide speed ranges. Such motors are being used in several applications, including nuclear power plants, the petroleum industry, water cooling systems, and the mining industry (Saad et al., 2018).

Despite their numerous advantages, the components of induction motor drive IMD are subjected to various types of faults during their operation which can lead to total damage of machine, which paralyzes the industrial process and therefore affects production. Some of them are related to the electrical machine including electrical fault either in the stator or wound rotor in the form of winding open or short circuit (Jannati et al., 2014),(Toma et al., 2013), broken bar fault in squirrel-cage rotor (Guellout et al., 2020),(Fernandez-Cavero et al., 2021), and mechanicalfailures, such as rotor bearingfault(Rezig et al., 2013),(Muthukumaran et al., 2021), air-gap eccentricityfault(Bagheri et al., 2020),(Zhou et al., 2021), faultsrelated to mechanical or electricalsensors(Liu et al., 2019),(Azzoug et al., 2021). Finally, failuresoccur in inverter power devices(Jian-Jian et al., 2019),(Cherif et al., 2019).Figure1 provides a simple classification of different faults that can affect the components of an AC motor drive.

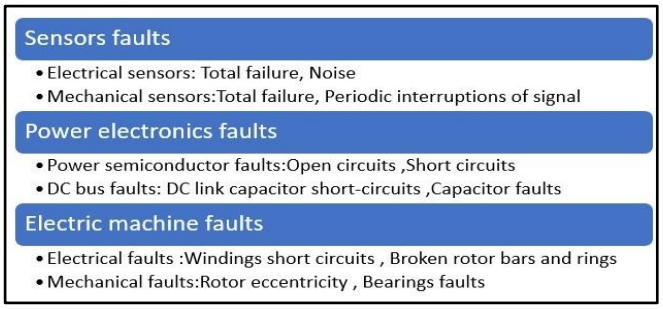

Figure.1. Classification of faults occurring in AC motor drive(Klimkowski & Dybkowski, 2016).

According to the statistics, the power converter faults cover about 80% of the different types of faults in electric motor drive applications (Orłowska-Kowalska et al., 2017). In (Chen et al., 2021), it is mentioned that the power converters faults are distributed as follows (see Figure 2): a power semiconductor device (21%), DC-link capacitor (30%), printed circuit boards (PCB) (26%), solder (13%), and others.

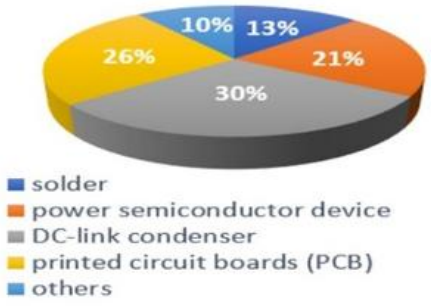

Figure.2. Faults distribution among power converter components.

Most voltage source inverters (VSI's) feeding AC motors use insulated gate bipolar transistors (IGBT's) as the power deviceswhich offer high switching frequency, high voltage,and current ratings, and high ability to handle short-circuit currents for periods exceeding 10 microseconds (Zdiri et al., 2019). Electrical fault types that may happen in IGBTs power devices can be categorized into Short Circuit Fault (SCF) and Open Switch Fault (OSF). This latter is not as dangerous as a short circuit fault and does not lead to the shutdown of the drive system and may remain undetected for an extended period of time. On the other hand, it may cause a secondary failure in the other components of the drive (Jorge Oliveira Estima, 2012). In this work, only OSF has been taken into consideration.

The diagnosis of the open-circuit faults of inverter power switches has become an important research topic. A variety of OSF diagnosis methods have been discussed in the literature for AC motor drives. These fault detection FD approaches have several classifications such as signal-based (FDSM) and model-based (FDMM) methods (Maamouri et al., 2018). A general block diagram of diagnostic methods for open switch failures is shown in Figure 3(Salehifar, 2014).

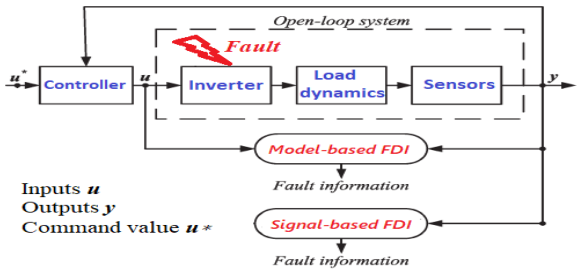

Figure.3.A general block diagram of the diagnostic methods for inverter open-transistor faults.

As regards the signal-based methods, current or voltage signals of the VSI are used to find the fault detection FD index. These methods offer fast fault detection and are independent of the system parameters (Chen et al., 2021). Many studies have been conducted on the implementation of signal-based diagnosis methods that concern open switch failures. In what follows, a review of some signal-based methods is presented.

Regarding the current-signal-based methods, an approach called Park's vector Method was suggested in (Mendes & Cardoso, 1999), its fault diagnosis process is achieved by computing the average value of the Park's vector currents in the complex (αβ) plan and the phase-angle. One drawback of this method is the load dependence. To make the fault detection algorithm independent from the load, another method called a Normalized DC Current Method was investigated in (Rothenhagen & Fuchs, 2005),(Rothenhagen & Fuchs, 2004) with the current fundamental component value being normalization quantity. As mentioned in (Rothenhagen & Fuchs, 2004), this method has some drawbacks in the case of closed-loop control systems. As a result, a Modified Normalized DC Current Method was proposed (Rothenhagen & Fuchs, 2005),(Rothenhagen & Fuchs, 2004). This latter uses the same algorithms as the Normalized DC Current method but employs a less restrictive way to locate the faulty switch. The same authors also proposed another version called "Simple Direct Current Method" that uses the mean phase current value for fault detection. Estima et al. proposed in (Jorge O. Estima & Cardoso, 2011) a new open switch fault detection method for PMSM drive based on average absolute values of phase currents, which allows for the diagnosis of single and multiple open-switch failures, also it is robust against false alarms. This approach has been later enhanced in (Zdiri et al., 2019) by adding other diagnostic variables. Another fault diagnosis method was discussed in (Jorge O. Estima & Marques Cardoso, 2013) in which the motor phase currents and their references were utilized to detect multiple open switch faults. In (Yan et al., 2018), the method based on average absolute values of phase currents is combined with a fuzzy logic approach to detect and locate single, multiple, and intermittent open circuit faults in power switches.

The open switch failures OSF diagnosis can also be performed by use of voltage. These methods have some good performances such as faster diagnosis speed, stronger independence of the load, and high robustness. However, as major weaknesses, they often require additional voltage sensors or extra hardware, so the implementation cost is high. Some examples of these methods are reported in (Sun et al., 2011),(Karimi et al., 2009),(Salehifar, 2014).

In this paper, we propose a novel fault detection and identification FDI method for vector controller of induction motor (IM) drive in the case of open-switch faults occurring in voltage source inverter. The faultdiagnosis process is only applied when the following faults appear: an opened phase fault and a single IGBT open-circuit fault. The rest of this paper is organized as follows. Section 2 describes the modeling and vector control strategy of a three-phase induction motor drive. The diagnosis method for an open switch faults OSF is detailed in Section 3. Simulation results for healthy and faulty operations are presented and discussed in Section 4. Finally, the conclusion is presented in Section 5.

2. Mathematical Model and Field-Oriented Controller of Induction Motor Drive

2.1 Induction Motor Mathematical Modelling

This section focuses on the mathematical analysis of the field-oriented controller (FOC) of a three-phase induction machine drive. Firstly, the mathematical model of a three-phase induction motor in *dq* reference frame fixed to the rotating magnetic field is expressed in vector form as follows(Zahraoui et al., 2016):

$$\frac{d}{dt}[X] = [A][X] + [B][U] \tag{1}$$

Where: $[X]$ stands for the state-variables vector,$[U]$ stands for the input vector. The components of each matrix are:

$$\mathrm{A} = \begin{bmatrix} -\gamma & \omega_s & \frac{k}{T_r} & kp\Omega \\ \omega_s & -\gamma & -kp\Omega & \frac{k}{T_r} \\ \frac{M}{T_r} & 0 & -\frac{1}{T_r} & (\omega_s - p\Omega) \\ 0 & \frac{M}{T_r} & -(\omega_s - p\Omega) & -\frac{1}{T_r} \end{bmatrix};\ \mathrm{B} = \begin{bmatrix} \frac{1}{\sigma L_s} & 0 \\ 0 & \frac{1}{\sigma L_s} \\ 0 & 0 \\ 0 & 0 \end{bmatrix};[X] = \begin{bmatrix} i_{sd} & i_{sq} & \psi_{rd} & \psi_{rq} \end{bmatrix}^t,\ [U] = \begin{bmatrix} u_{sd} & u_{sq} \end{bmatrix}^t$$

Where: $T_r = \frac{L_r}{R_r}; \sigma = 1 - \frac{M^2}{L_s L_r}; \gamma = \frac{R_s}{\sigma L_s} + \frac{1-\sigma}{\sigma T_r}; k = \frac{1-\sigma}{\sigma M}$

The quantities i_{sd} , i_{sq} , u_{sd} , u_{sq}, R_s , L_s, M correspond to stator direct axis current, stator quadrature axis current, stator direct axis voltage stator, stator quadrature axis voltage, stator resistance, stator self-inductance, and magnetizing inductance, respectively. Also, ψ_{rd} , ψ_{rq}, R_r , L_r are direct axis rotor flux linkage, quadrature axis rotor flux linkage, rotor resistance, and rotor self-inductance, respectively.

The electromechanical torque developed by IM is given by the following expression:

$$T_{em} = \frac{3}{2} p \frac{M}{L_r} \left(i_{sq}\ \psi_{rd} - i_{sd}\ \psi_{rq} \right) \tag{2}$$

2.2 Induction Motor Control Strategy

The three-phase induction motor drive is controlled using the indirect field-oriented control (IFOC) strategy as shown in Figure 4. The inputs of the IFOC block are, the reference torque T_e^* generated by the PI speed controller, and the flux command ψ_{rd}^* considered constant. The outputs of IFOC are given by the following expressions:

- Sleep frequency ω_{sl}:

$$\omega_{sl} = \frac{M}{T_r} \frac{i_{sq}^*}{\psi_{rd}^*} \tag{3}$$

- The references stator currents in *dq* reference frame are as follows:

$$i_{sd}^* = \frac{\psi_{rd}^*}{M},\ \ i_{sq}^* = \frac{L_r T_e^*}{pM \psi_{rd}^*} \tag{4}$$

- The synchronous frequency ω_s and the rotor flux θ_s angle are given from:

$$\omega_s = \omega_{sl} + p\Omega\,, \quad \theta_s = \int \omega_s dt \tag{5}$$

Where Ω is the mechanical speed.

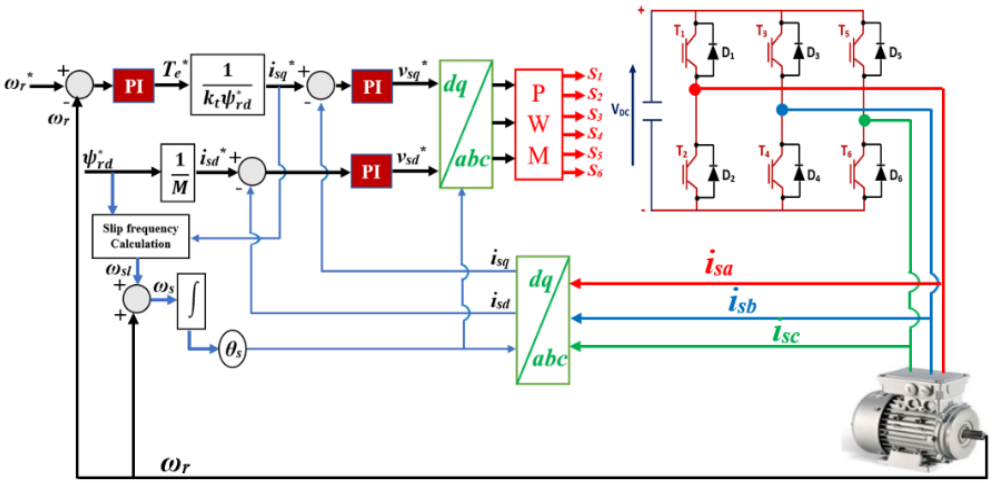

Figure.4. Block diagram of the indirect field-oriented controller IFOC applied to IM.

3. Fault Diagnosis Method

3.1 Open-Switch Fault in Standard IM Drive

The induction motor in healthy operation is supplied by a two-level voltage source inverter (VSI), whose circuit topology is presented in Figure 5. The switching states of the six insulated gate bipolar transistors IGBTs power switches (T1-T6) of the inverter are represented by the binary variables Si (*i=1-6*), where the value "1" corresponds to an ON state and the binary "0" indicates an OFF state (El Badsi et al., 2013). The command signals for the upper and bottom IGBTs on the same leg are complementary: $S_{i+1} = \overline{S_i}$, *i*=1,3,5. Where Vdc is the dc-link voltage.

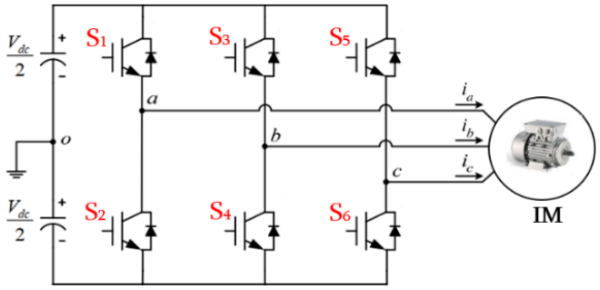

Figure.5. Three-phase standard inverter (VSI) fed an induction motor.

When an IGBT open-circuit fault occurs, the phase currents become an unbalanced three-phase system. This significant distortion of the phase currents causes the appearance of electromagnetic torque ripples. Generally, such a fault does not cause an IM-drive shutdown but degrades its performance. The effect of OSF is clearly visible if studying the phase currents in a fixed frame called the Current vector trajectory. The *abc*-phase currents are transformed to a stationary two-phase reference frame using Clarke transformation. Consequently, the αβ currents components are expressed according to:

$$\begin{bmatrix} i_{s\alpha} \\ i_{s\beta} \end{bmatrix} = \sqrt{\frac{2}{3}} \begin{bmatrix} 1 & -0.5 & -0.5 \\ 0 & -\frac{\sqrt{3}}{2} & -\frac{\sqrt{3}}{2} \end{bmatrix} \begin{bmatrix} i_{sa} \\ i_{sb} \\ i_{sc} \end{bmatrix} \tag{6}$$

In the case of a healthy operating inverter, vector trajectory has a circle shape as shown in Figure 6(a). A change in the shape of this trajectory is an indicator of the occurrence of an open switch fault. The ideal shape of

different trajectories of the phase current according to the faulty switch is illustrated in Figure 6(b)(Orlowska-Kowalska & Sobański, 2015).

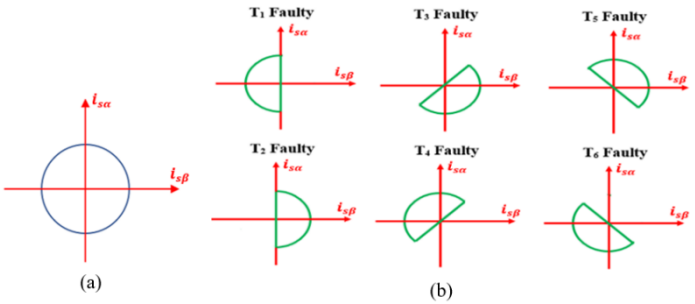

Figure.6. Current vector trajectory according to faulty switches in the 2-level VSI (a)Normal condition, (b) Faulty condition.

3.2 Diagnosis of Open-Switch Faults

The main idea of the proposed diagnostic approach is to use the measured stator currents (i_{sa}, i_{sb},i_{sc}) as inputs signals for FDI unit. These currents are also used in the vector control algorithm (see Figure 4) which leads to avoiding the use of additional sensors, decreases the cost of the hardware system, and increases the reliability of the system. Generally, when one of the IGBT does not turn *ON*, in the case of motor operation, current in that phase is zero for a half cycle, either positive half cycle or negative half depending on whether it is upper IGBT *Ti*(i=1,3,5) or lower IGBT *Tj*(j=2,4,6).This information will be used to construct the diagnostic method discussed below.

Figure 7 illustrates a block diagram of the FDI algorithm. The inputs of this block are the i_{sk}(k = *a*, *b*, *c*) that represents the *a*- phase, *b*- phase, and *c*- phase measured currents, and the output is the faulty switch T_i^f (i = 1:6).

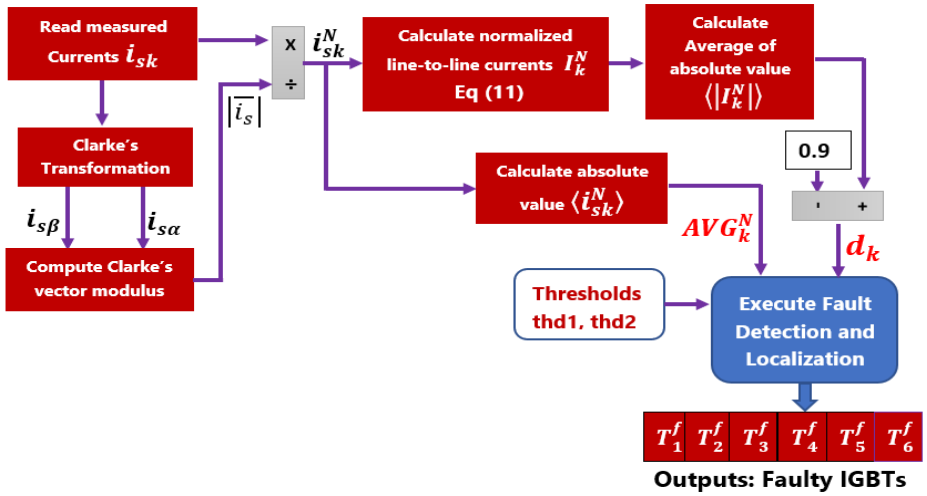

Figure.7. Block diagram of the proposed open switch fault diagnosis (FDI) method.

According to Figure 7, the proposed fault diagnosis method consists of two steps. The first one concerns the detection of the leg, which contains the faulty switch, it is based on the computing of the average of the absolute value of normalized line to line currents. In the next step, the identification of faulted switch(T_i^f) is achieved by using the average of the absolute value of normalized phase currents.

A. Detection of An Open Switch Fault

When the induction motor is powered by a healthy voltage source inverter VSI, the three-phase symmetrical current waveforms are defined by the following equations:

$$\begin{cases} i_{sa}(t) = I_m \sin(\omega_s t) \\ i_{sb}(t) = I_m \sin\left(\omega_s t - \frac{2\pi}{3}\right) \\ i_{sc}(t) = I_m \sin\left(\omega_s t + \frac{2\pi}{3}\right) \end{cases} \quad (7)$$

where $I_m$is the three-phase current amplitude, $\omega_s$is the angular frequency.

In faulty operation, assuming an open circuit fault occurs in the bottom IGBT of leg-*b*, the current of phase-*b* during one fundamental period can be given by:

$$i_{sb}(t) = \begin{cases} I_m sin\left(\omega_s t - \frac{2\pi}{3}\right) if \quad \frac{2\pi}{3\omega_s} < t \le \frac{5\pi}{3\omega_s} \\ 0 \quad if \quad \frac{5\pi}{3\omega_s} < t \le \frac{8\pi}{3\omega_s} \end{cases} \quad (8)$$

In order to make the FDI algorithm overcome the impact of load change, the current of each phase is normalized using Clarke's vector modulus defined as follows:

$$\left|\overline{i_s}\right| = \sqrt{i_{s\alpha}^2 + i_{s\beta}^2} = I_m \sqrt{\frac{3}{2}} \quad (9)$$

Where the currents ($i_{s\alpha}$,$i_{s\beta}$) in a fixed (αβ) two-axis frame are predefined in (6):
Through Clarke's vector modulus given in (9), the normalized currents (i_{sk}^N) are given by the following formulas:

$$i_{sk}^N = \frac{i_{sk}}{\left|\overline{i_s}\right|} = \begin{cases} i_{sa}^N = \sqrt{\frac{2}{3}} \sin(\omega_s t) \\ i_{sb}^N = \sqrt{\frac{2}{3}} \sin\left(\omega_s t - \frac{2\pi}{3}\right) \\ i_{sc}^N = \sqrt{\frac{2}{3}} \sin\left(\omega_s t + \frac{2\pi}{3}\right) \end{cases} \quad (10)$$

According to (10), the normalized currents i_{sk}^N (*k*=a,b,c) are balanced sinusoidal currents and take values within the range of ± 0.8165.

Now, we define new quantities, which are the normalized line-to-line currents expressed as follows:

$$\begin{cases} I_a^N = i_{sb}^N - i_{sc}^N = -\sqrt{2}\cos(\omega_s t) \\ I_b^N = i_{sc}^N - i_{sa}^N = +\sqrt{2}\cos\left(\omega_s t + \frac{\pi}{3}\right) \\ I_c^N = i_{sa}^N - i_{sb}^N = +\sqrt{2}\cos\left(\omega_s t - \frac{\pi}{3}\right) \end{cases} \quad (11)$$

The average absolute values of the three normalized line-to-line currents $\langle |I_k^N| \rangle$ under no-fault operation are given by:

$$\left\langle \left| I_k^N \right| \right\rangle = \frac{\omega_s}{\pi} \int_0^{\frac{\pi}{\omega_s}} \left| \sqrt{2}\cos\left(\omega_s t + \frac{\pi}{3}\right) \right| dt \approx 0.9 \quad (12)$$

where <> is signal average value at fundamental frequency.

The approximatevalues of $\langle |I_k^N| \rangle$in the case of a single open switch or an open-circuit fault of leg-*k* (*k*=a,b,c) are listed in **Table 1**:

Table.1. Average absolute values of the three normalized line-to-line currents under a single open switch and open phase faults.

Average absolute values	Faulty Switches								
	T1	T2	T3	T4	T5	T6	T1, T2	T3, T4	T5, T6
$\langle\lvert I_a^N\rvert\rangle$	1.15	1.15	0.8	0.8	0.8	0.8	1.4	0.7	0.7
$\langle\lvert I_b^N\rvert\rangle$	0.8	0.8	1.15	1.15	0.8	0.8	0.7	1.4	0.7
$\langle\lvert I_c^N\rvert\rangle$	0.8	0.8	0.8	0.8	1.15	1.15	0.7	0.7	1.4

Based on the above analysis, we define the first fault indicator named the detection variables d_k as follows:

$$d_k = \left\langle \left| I_k^N \right| \right\rangle - 0.9 \tag{13}$$

The behavior of the detection variables varies according to the VSI state. When the drive works normally, all the detection variables d_k are close to zero. However, if an OSF fault happens in the upper or lower IGBT of leg-*k*, the corresponding fault detection variable is near to 0.25, whereas it is close to -0.1 for the healthy legs. In addition,d_k increases immediately to the value 0.5 when an open-circuit fault occurs in leg-*k*.By the combination of the diagnostic variables d_k and the fault detection thresholds (*thd1, thd2*), the detection of a single open switch faultor leg open-circuit fault is performed using the following algorithm:

$$D_k\big|_{\text{k=a,b,c}} = \begin{cases} N & \text{if } d_k < 0 \\ 0 & \text{if } d_k = 0 \\ P & \text{if } th_{d1} \le d_k < th_{d2} \\ PP & \text{if } d_k \ge th_{d2} \end{cases} \tag{14}$$

When D_k =0, it means the healthy operation mode. However, when D_k takes a positive value *P* there is an open switch fault in the leg-*k*, and if D_k takes a value *PP*, it is the case of a leg-*k* open-circuit fault.

B. Identification of an Open Switch Fault

The variable D_k does not allow the localization of a faulty switch, it just carries information about the affected leg, so we will define an identification variable AVG_k^N based on the calculation of the average value of the normalized three-phase currents (Yan et al., 2018). The fault identification variables can be formulated according to the following relationship:

$$AVG_k^N\big|_{\text{k=a,b,c}} = \begin{cases} L & \text{if } \left\langle i_k^N \right\rangle < 0 \quad \text{upper switch fault} \\ H & \text{if } \left\langle i_k^N \right\rangle > 0 \quad \text{lower switch fault} \end{cases} \tag{15}$$

Under healthy VSI conditions, all identifications variables AVG_k^N are approximately equal to zero. However, when an OSF occurs in leg-*k*, if the corresponding identification variable is negative '*L*' then the upper switch*Ti*(*i=1,3,5*) is the faulty component. Otherwise, the lower switch *Tj*(*j=2,4,6*) is the faulty component. In addition, if the absolute average value is equal to zero during one period, the fault type is the open phase.

Finally, by using together with the detection variables D_k defined in (14) and the identification ones AVG_k^N given in (15), the localization of the faulted IGBTs (upper, lower, or for two IGBTs in the same leg) is achieved through the fault identification flags $F_k$described as follows:

$$F_k\big|_{k=a,b,c} = \left\{ \begin{array}{cc} 1 & OSF\ T_i \\ -1 & OSF\ T_{i+1} \\ 2 & OSF\ T_i\ \&T_{i+1} \end{array} \right|_{i=1,3,5} \tag{16}$$

The fault flags F_k are 1, -1, and 2 in the case of upper switch fault, lower switch fault, and open-phase fault, respectively.

Based on the above analysis, by using the fault detection variables D_k,fault identification variables AVG_k, and fault identification flags F_k(*k = a, b, c)* the detection and location of either an open-switch fault or an open phase fault is shown in **Table 2**.

Table.2. The relationship between diagnosis variables and faulty switches.

		Diagnosis variables ***i=1,2,3 and k=a,b,c***		
Fault type	**Faulty switch**	D_k	AVG_k^N	F_k
Single open switch	Normal	0	0	0
	T_i	P	L	1
	T_{i+1}	P	H	-1
Open phase	T_i and T_{i+1}	PP	0	2

4. Simulation Results and Comments

In this section, we provide a series of computer simulations using MATLAB/Simulink environment to verify the effectiveness of the suggested FDI method. The IM was controlled by the field-oriented vector control strategy. The parameters of the induction motor and the VSI are stated in **Table 3**.

Table.3. The induction motor and VSI parameters

Induction motor	
Rated speed *Nn*	1400 rpm
Rated power *Pn*	1.5 kW
Voltage*V*	380 V
Line current	6.3 A
Phase current	3.6 A
Rated frequency*f*	50 Hz
Stator inductance*Ls*	0.39 H
Mutual inductance*M*	0.47 H
Rotor inductance*Lr*	0.61 H
Stator resistance*Rs*	5.43Ω
Rotor resistance*Rr*	3.59 Ω
Moment of inertia*J*	0.027 kg.m^2
Pole pairs*p*	2
Voltage source inverter VSI	
DC-link voltage*Vdc*	540 V
PWM switching frequency*fs*	1650 Hz

4.1 IM Drive Under IGBT Open Circuit Fault

The simulation of an OSF is achieved by setting the gate drive signals to null as shown in Figure 8:

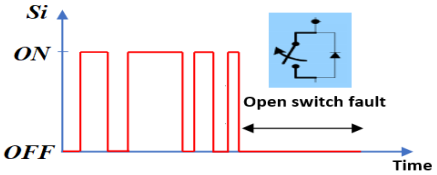

Figure.8. Simulation of an IGBT open circuit fault.

- Fault 1: An OSF occurs in the upper switch T1 of leg-a at *tf*=0.7 sec for a speed reference of 700 rpm and under 50% of the motor rated torque applied at t_L = 0.4 sec.
- Fault 2: Faults occur in the switches T3 and T4 of leg-b simultaneously at *tf*=0.7 sec where the speed reference is set to 1200 rpm and under 70% of the motor rated torque applied at t_L = 0.4 sec.

Figures 9 and 10indicate the responses of the IM-drive in terms of phase currents, motor speed, and torque for the two cases of fault. Firstly, from Figures 9(a) and 10(a), when the IM-drive operates under healthy conditions, the phase currents have sinusoidal waveforms. Once the fault occurs at *tf*=0.7 sec in T1, the current of phase-a is limited to flow only in the negative direction. Regarding fault 2, the control signals are removed from both switches (T3, T4) at *tf*=0.7 sec, which leads to an opening-circuit fault of the phase-b.

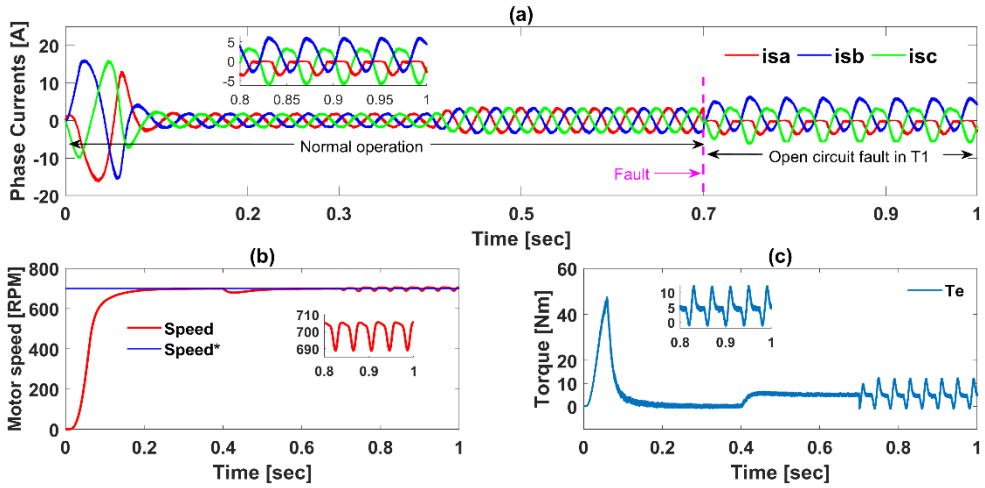

Figure.9. Simulation results of an open circuit fault in T1 of phase-a (Fault 1) with 700 rpm and 50% of load torque. (a) Phase currents (b) Mechanical Speed (c) Torque.

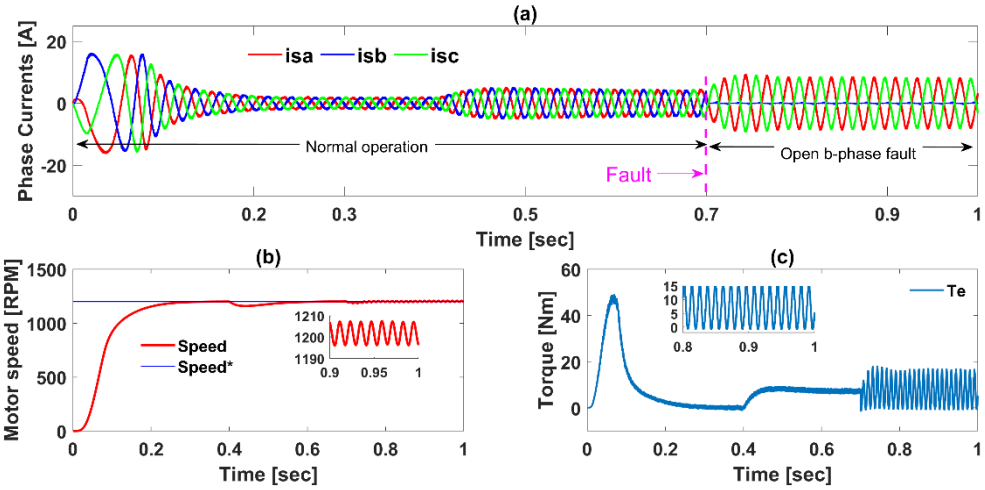

Figure.10. Simulation results for a fault in T3 and T4 of phase-b (Fault 2) with 1200 rpm and 70% of load torque. (a) Phase currents (b) Mechanical Speed (c) Torque.

Figures 9(b,c), and 10(b,c) show the time-domain variations of motor speed and torque. It is possible to observe that the speed and torque are affected, and exhibit ripples as soon as a fault occurs. In the event of fault 2, the motor will be supplied only by two phases, which causes fast ripples in speed and electromagnetic torque.

4.2 Fault Detection and Identification Variables

In this section, the simulation results are achieved to verify the proposed FDI algorithm against either an open circuit switch fault (upper switch T3 and, lower switch T2) or an open *c*-phase fault. The fault diagnosis results are presented in Figures 11,12 and 13. For both healthy and faulty operating conditions, a speed reference has been taken equal to 1000 rpm and considering a load torque equal to 50% of the rated one. The OSF detection threshold values *thd1* and *thd2*for (14) are set to be equal to 0.2 and 0.23 respectively.

From Figures 11,12 and 13, under normal operation of IM-drive, it is observed that the phase-currents have sinusoidal waveforms, which gets a null value for the diagnostic variables *Dk*, *AVGk*, and flags *Fk*.

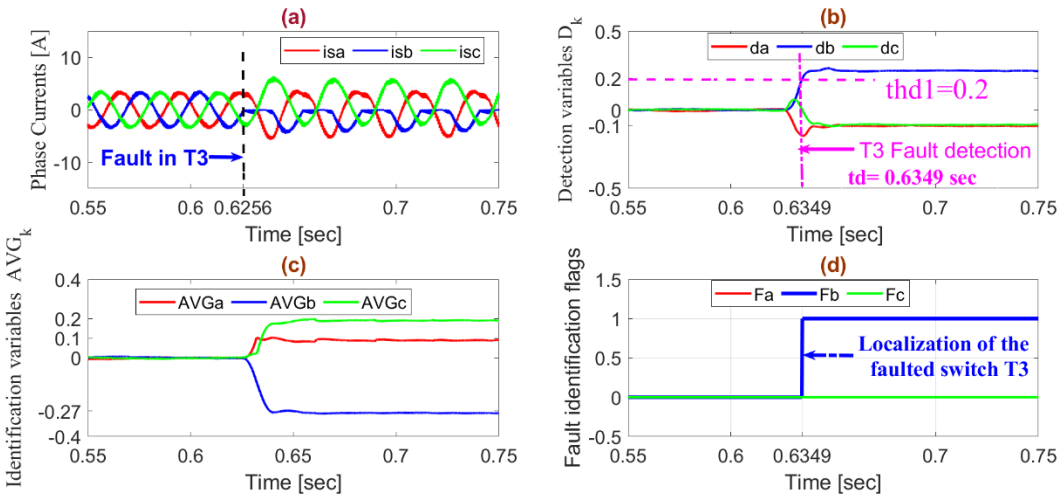

Figure.11. Diagnosis results for an OSF fault in T3 under 5 Nm load torque and for a reference speed of 1000 rpm. (a) Phase currents (b) Fault detection variables (c) Identification variables (d) Identification flags.

Concerning results in Figure 11, after an open-circuit fault happens in T3 at *tf*=0.6256 sec, the positive half-wave of the b-phase current becomes equal to zero. As a result, the detection variable *db*increases to converge approximately to near 0.25, exceeding the threshold *thd1* at the instant *td*= 0.6349 sec, and ones related to the healthy phases *da* and *dc* decrease to reach the value of about -0.1 as indicated in Figure 11(b). In addition, as shown in Figure 11(d), the identification flag *Fb*becomes equal to +1 (whereas *Fa*= 0, *Fc* = 0) under the fault operation, allowing for the identification of the faulty switch T3. According to **Table.2** and equations (14)-(16), the open switch fault of T3 is detected and identified at time *td*= 0.6349 sec, which gives a detection speed equivalent to 31.13 % of the phase currents fundamental period.

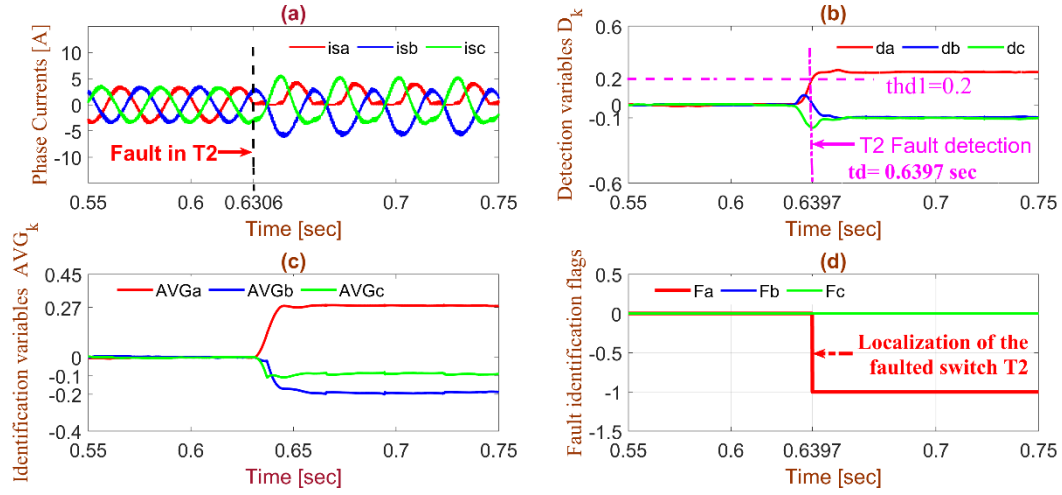

Figure.12. Diagnosis results for an OSF fault in T2 under 5 Nm load torque and for a reference speed of 1000 rpm. (a) Phase currents (b) Fault detection variables (c) Identification variables (d) Identification flags.

Other diagnostic results are shown in Figure 12 where an open-circuit fault in the lower IGBT T2 of the second inverter-leg is applied at *tf*=0.6306 sec. Before the fault occurrence, concerning the currents and the diagnostic variables, the same remarks as in the previous case were observed. After the fault occurs, the detection variable related to faulted phase *da* quickly changes and breaks through the threshold *thd1* at 0.6397 sec. As a result, the identification flag *Fa* decreases immediately from 0 to -1 at 0.6397 sec (and *Fb* = 0, *Fc* = 0) allowing for the identification of the faulty switch T2 as indicated in Figure 12(d). So, from the above information, the detection and localization of the faulty IGBT T2 are achieved after approximately 9*msec* of the fault occurrence, which corresponds approximatively to 30.43 % of the phase currents fundamental period.

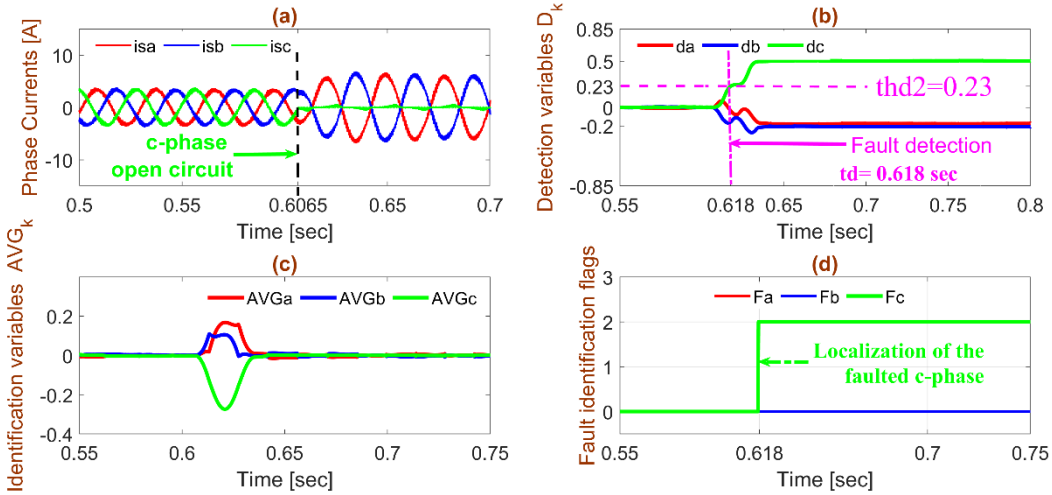

Figure.13. Diagnosis results when T5 and T6 are under open-circuit fault. (a) Phase currents (b) Fault detection variables (c) Identification variables (d) Identification flags.

Next, the fault diagnosis process is also applied for an open phase fault as shown in Fig. 13. The switching signals of IGBTs T5 and T6 have been removed simultaneously at *tf*= 0.6065 sec. When the detection variable *dc* corresponding to the affected phase exceeds the predefined threshold value *thd2* at *td*= 0.618 sec, the fault identification flags (*Fa Fb Fc*) change from (000) to (001), as shown in Figure 13(b) and Figure 13(d). As a result, the diagnosis method for this kind of fault (open phase fault) takes about 37 % of the fundamental current period to identify the faulted phase.

4.3 FDI Robustness Against Speed and Load Torque Transients

The precise selection of fault detection thresholds *(thd1*, *thd2*) is an important task because it has a significant impact on the diagnosis method's robustness and immunity in healthy operation (Gmati et al., 2021). In this work, thethreshold value is selected by studying the behavior of the detection variables *Dk* for normal and All faulty operations of IM-drive. A trade-off between a quick diagnosis process and robustness against false alarms is also considered. A higher threshold value increases the fault detection time while making the FDI scheme even more robust against transients. On the contrary, a lower threshold value makes the detection method vulnerable to false alarms.

To check the robustness of the proposed FDI algorithm against speed and load torque variations,two transient states were applied to the FDI block. Figure14 shows the simulation results of the time-domain waveforms of the motor phase currents together with the fault detection variables during transients caused by the change in mechanical load and motor speed. A speedand load variations versus time are as follows:

- The reference speed is set to 700 rpm in t = 0 − 0.6 sec, and then it is increased to 1000 rpm at t = 0.6sec and finally increases to 1300 rpm at t = 0.8 sec.
- At t =0.3 sec the load torque increase from 2 to 8 Nm (20% to 80% of the rated torque), and then it isincreased to 10 Nm (100% of the rated torque) at t = 0.5 sec.

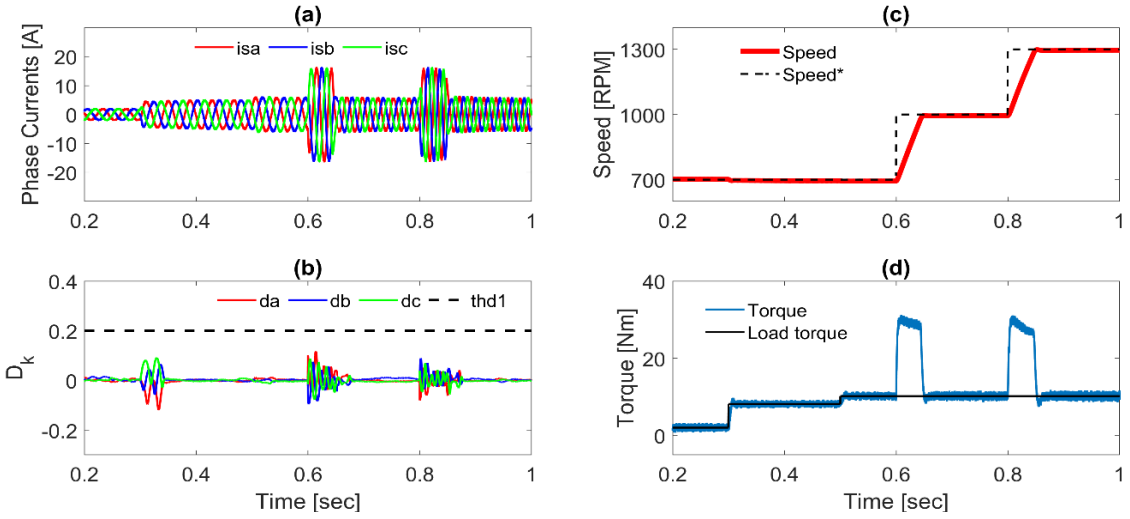

Figure.14. Simulation results under load and speed changes.
(a) phase currents (b) detection variables (c) speed (d) torque.

It can be seen from these results that during this change in mechanical load and speed, the detection variables undergo a light deformation, but it does not exceed the thresholds *thd1=0.2* and *thd2=0.23*. As a result, there are no false alarms generated in the FDI process.

5. Conclusion

This paper proposes a new FDI signal-based method concerning open switch faults of a three-phase inverter feeding an induction motor controlled by field-oriented control FOC strategy. The FDI algorithm uses phase currents as diagnostic signals already used in the vector controller algorithm, which leads to avoiding the use of additional sensors.Thus, it is a cost-effective method. Firstly, the absolute average value of the normalized line to line currents is used to determine the fault detection variables. After that, the identification of the faulty IGBT is achieved by calculating the average value of the normalized phase currents.

The simulation results show that the proposed diagnosis algorithm presents interesting performances in terms of fast fault detection time, robustness against transients caused by variations in speed and load torque.

Concerning the fault detection time, less than half of the fundamental period is required to locate the fault; about 30.5-31.5% and 36-37% of an electrical period for an open switch fault and an open phase faultrespectively. The performance improvement of this method as well as its experimental validation will be our future work.

References

Azzoug, Y., Sahraoui, M., Pusca, R., Ameid, T., Romary, R., & Marques Cardoso, A. J. (2021). Current sensors fault detection and tolerant control strategy for three-phase induction motor drives. *Electrical Engineering*, *103*(2). https://doi.org/10.1007/s00202-020-01120-5

Bagheri, A., Ojaghi, M., & Bagheri, A. (2020). Air-gap eccentricity fault diagnosis and estimation in induction motors using unscented Kalman filter. *International Transactions on Electrical Energy Systems*, *30*(8), e12450. https://doi.org/10.1002/2050-7038.12450

Chen, T., Pan, Y., & Xiong, Z. (2021). Fault diagnosis scheme for single and simultaneous open‐circuit faults of voltage‐source inverters on the basis of fault online simulation. *Journal of Power Electronics*, *21*(2), 384–395. https://doi.org/10.1007/s43236-020-00209-1

Cherif, B. D. E., Bendiabdellah, A., Bendjebbar, M., & Tamer, A. (2019). Neural network based fault diagnosis of three phase inverter fed vector control induction motor. *Periodica Polytechnica Electrical Engineering and Computer Science*, *63*(4). https://doi.org/10.3311/PPee.14315

El Badsi, B., Bouzidi, B., & Masmoudi, A. (2013). DTC scheme for a four-switch inverter-fed induction motor emulating the six-switch inverter operation. *IEEE Transactions on Power Electronics*, *28*(7). https://doi.org/10.1109/TPEL.2012.2225449

Estima, Jorge O., & Cardoso, A. J. M. (2011). A new approach for real-time multiple open-circuit fault diagnosis in voltage-source inverters. *IEEE Transactions on Industry Applications*, *47*(6). https://doi.org/10.1109/TIA.2011.2168800

Estima, Jorge O., & Marques Cardoso, A. J. (2013). A new algorithm for real-time multiple open-circuit fault diagnosis in voltage-fed PWM motor drives by the reference current errors. *IEEE Transactions on Industrial Electronics*, *60*(8), 3496–3505. https://doi.org/10.1109/TIE.2012.2188877

Estima, Jorge Oliveira. (2012). *Development and Analysis of Permanent Magnet Synchronous Motor Drives with Fully Integrated Inverter Fault-Tolerant Capabilities* [Ph.D. dissertation]. Coimbra Univ.

Fernandez-Cavero, V., Pons-Llinares, J., Duque-Perez, O., & Morinigo-Sotelo, D. (2021). Detection of Broken Rotor Bars in Nonlinear Startups of Inverter-Fed Induction Motors. *IEEE Transactions on Industry Applications*, *57*(3). https://doi.org/10.1109/TIA.2021.3066317

Gmati, B., Jlassi, I., Khojet El Khil, S., & Marques Cardoso, A. J. (2021). Open-switch fault diagnosis in voltage source inverters of PMSM drives using predictive current errors and fuzzy logic approach. In *IET Power Electronics* (Vol. 14, Issue 6). https://doi.org/10.1049/pel2.12098

Guellout, O., Rezig, A., Touati, S., & Djerdir, A. (2020). Elimination of broken rotor bars false indications in induction machines. *Mathematics and Computers in Simulation*, *167*, 250–266. https://doi.org/10.1016/j.matcom.2019.06.010

Jannati, M., Monadi, A., Idris, N. R. N., & Aziz, M. J. A. (2014). Speed sensorless vector control of unbalanced three-phase induction motor with adaptive sliding mode control. *International Journal of Power Electronics and Drive Systems*, *4*(3), 406–418. https://doi.org/10.11591/ijpeds.v4i3.6212

Jian-Jian, Z., Yong, C., Zhang-Yong, C., & Anjian, Z. (2019). Open-Switch Fault Diagnosis Method in Voltage-Source Inverters Based on Phase Currents. *IEEE Access*, *7*(c), 63619–63625. https://doi.org/10.1109/ACCESS.2019.2913164

Karimi, S., Poure, P., & Saadate, S. (2009). Fast power switch failure detection for fault tolerant voltage source inverters using FPGA. *IET Power Electronics*, *2*(4). https://doi.org/10.1049/iet-pel.2008.0075

Klimkowski, K., & Dybkowski, M. (2016). A fault tolerant control structure for an induction motor drive system.

Automatika, *57*(3), 638–647.

Liu, Y., Stettenbenz, M., & Bazzi, A. M. (2019). Smooth Fault-Tolerant Control of Induction Motor Drives with Sensor Failures. *IEEE Transactions on Power Electronics*, *34*(4), 3544–3552. https://doi.org/10.1109/TPEL.2018.2848964

Maamouri, R., Trabelsi, M., Boussak, M., & M'Sahli, F. (2018). Fault Diagnosis and Fault Tolerant Control of a Three-Phase VSI Supplying Sensorless Speed Controlled Induction Motor Drive. *Electric Power Components and Systems*, *46*(19–20), 2159–2173. https://doi.org/10.1080/15325008.2018.1534899

Mendes, A. M. S., & Cardoso, A. J. M. (1999). Fault diagnosis in a rectifier-inverter system used in variable speed ac drives by the average current Park's vector approach. *European Power Electronics Conference*, 1–9.

Muthukumaran, S., Rammohan, A., Sekar, S., Maiti, M., & Bingi, K. (2021). Bearing fault detection in induction motors using line currents. *ECTI Transactions on Electrical Engineering, Electronics, and Communications*, *19*(2). https://doi.org/10.37936/ECTI-EEC.2021192.244163

Orłowska-Kowalska, T., Kowalski, C. T., & Dybkowski, M. (2017). Fault-diagnosis and fault-tolerant-control in industrial processes and electrical drives. In *Studies in Systems, Decision and Control* (Vol. 75, pp. 101–120). Springer. https://doi.org/10.1007/978-3-319-45735-2_5

Orlowska-Kowalska, T., & Sobański, P. (2015). Simple diagnostic technique of a single IGBT open-circuit faults for a SVM-VSI vector controlled induction motor drive. *Bulletin of the Polish Academy of Sciences. Technical Sciences*, *63*(1).

Rezig, A., N'Diye, A., Djerdir, A., & Mekideche, M. R. (2013). Experimental investigation of vibration monitoring technique for online detection of bearing fault in induction motors. *Journal of Electromagnetic Waves and Applications*, *27*(4), 496–506. https://doi.org/10.1080/09205071.2013.753662

Rothenhagen, K., & Fuchs, F. W. (2005). Performance of diagnosis methods for IGBT open circuit faults in three phase voltage source inverters for AC variable speed drives. *2005 European Conference on Power Electronics and Applications*, *2005*. https://doi.org/10.1109/epe.2005.219426

Rothenhagen, K., & Fuchs, F. W. (2004). Performance of diagnosis methods for IGBT open circuit faults in voltage source active rectifiers. *2004 IEEE 35th Annual Power Electronics Specialists Conference (IEEE Cat. No. 04CH37551)*, *6*, 4348–4354.

Saad, N., Irfan, M., & Ibrahim, R. (2018). Condition Monitoring and Faults Diagnosis of Induction Motors. In Taylor & Francis Group (Ed.), *Condition Monitoring and Faults Diagnosis of Induction Motors* (1st ed.). CRC Press. https://doi.org/10.1201/9781351172561

Salehifar, M. (2014). *Fault diagnosis and fault tolerant control of multiphase voltage source converters for application in traction drives* [Ph.D. dissertation]. Catalonia Polytechnic Univ.

Sun, L., An, Q. T., Sun, L. Z., & Zhao, K. (2011). Switching function model-based fast-diagnostic method of open-switch faults in inverters without sensors. *IEEE Transactions on Power Electronics*, *26*(1). https://doi.org/10.1109/TPEL.2010.2052472

Toma, S., Capocchi, L., & Capolino, G. A. (2013). Wound-rotor induction generator inter-turn short-circuits diagnosis using a new digital neural network. *IEEE Transactions on Industrial Electronics*, *60*(9), 4043–4052. https://doi.org/10.1109/TIE.2012.2229675

Yan, H., Xu, Y., Cai, F., Zhang, H., Zhao, W., & Gerada, C. (2018). PWM-VSI Fault Diagnosis for a PMSM Drive Based on the Fuzzy Logic Approach. *IEEE Transactions on Power Electronics*, *34*(1), 759–768. https://doi.org/10.1109/TPEL.2018.2814615

Zahraoui, Y., Fahassa, C., Akherraz, M., & Bennassar, A. (2016). Sensorless vector control of induction motor using an EKF and SVPWM algorithm. *2016 5th International Conference on Multimedia Computing and Systems (ICMCS)*, 588–593.

Zdiri, M. A., Bouzidi, B., & Hadj Abdallah, H. (2019). Performance investigation of an advanced diagnostic method for SSTPI-fed IM drives under single and multiple open IGBT faults. *COMPEL - The International Journal for Computation and Mathematics in Electrical and Electronic Engineering*, *38*(2), 616–641. https://doi.org/10.1108/COMPEL-04-2018-0181

Zhou, L., Wang, B., Lin, C., Inoue, H., & Miyoshi, M. (2021). Static Eccentricity Fault Detection for PSH-type Induction Motors Considering High-order Air Gap Permeance Harmonics. *2021 IEEE International Electric Machines and Drives Conference, IEMDC 2021*. https://doi.org/10.1109/IEMDC47953.2021.9449496